





Water triggered injectable polylactic acid hydrogel based on zwitterionic sulfobetaine modification for incompressible bleeding and tissue anti-adhesion

Xinran Yang^{a,b,c} , Xiudan Wang^{a,b,c}, Lizong Tang^{a,b,c}, Zhiguang Sun^{a,b,c},
Xing Gao^{a,d}, Yanmei Zhao^{a,b,c}, Shike Hou^{a,b,c,**}, Jie Shi^{a,b,c,***},
Qi Lv^{a,b,c,*} 

^a Institution of Disaster and Emergency Medicine, Tianjin University, Tianjin, 300072, China

^b Key Laboratory for Disaster Medicine Technology, Tianjin, 300072, China

^c Wenzhou Safety (Emergency) Institute of Tianjin University, Wenzhou, 325026, China

^d Tianjin Hospital, Tianjin University, Tianjin, 300072, China

ARTICLE INFO

Keywords:

Injectable hydrogel
Zwitterion
Anti-adhesion
Incompressible bleeding
Hemostasis

ABSTRACT

Massive blood loss is the main cause of prehospital trauma-related death, the development of rapid and effective hemostatic materials is imminent. Injectable hydrogels have the advantages of covering irregular bleeding sites and quickly closing the wound. However, its inherent viscosity can easily precipitate tissue adhesion *in vivo* and other complications. Based on the anti-protein properties of zwitterion and our previous work about *in situ* hemostatic/anti-adhesion hydrogel material, we have synthesized a series of injectable hydrogel composed of sulfobetaine-modified polylactic acid (PLA) and gelatin (Gel). These hydrogels could form a smooth film structure by simple water triggering, thereby conferring anti-adhesive properties. We visualized the changes in surface hydrophobicity using fluorescent probes and demonstrated tissue adhesion, rapid hydrophobic interface response, as well as rapid hemostasis for incompressible wounds through *in vivo* and *in vitro* experiments. Additionally, we explored the application of hydrogel materials in the scenario of postoperative bleeding, which can effectively prevent unnecessary adhesion through rapid film formation and the anti-protein property of sulfobetaine. We believe that this multifunctional hemostatic hydrogel has the potential to serve as a prehospital emergency treatment of incompressible bleeding and benefit to the postoperative recovery of patients.

1. Introduction

Hemorrhagic shock remains the second-leading cause of early mortality among trauma victims, with uncontrolled bleeding and hemorrhagic shock accounting for 30–40 % of trauma-related deaths [1]. Timely intervention after injury is crucial to control bleeding in order to minimize early fatalities. Traditional methods such as gauze or tourniquets often fall short in managing incompressible bleeding and emergency blood transfusions or surgical intervention is required [2]. However, these methods can be challenging to implement swiftly in emergency scenarios, underscoring the need for further research into pre-hospital first aid for incompressible bleeding.

Injectable hydrogels with robust adhesion ability can adapt to the irregular wound shape and rapidly bind to the wound. Subsequently, hemostasis can be achieved through the formation of physical barriers and the triggering of coagulation cascades [3]. Pan et al. [4] prepared a dual biomimetic hydrogel based on mussel and barnacle cement proteins, the hydrogel can achieve strong wet tissue adhesion properties and effective sealing hemostasis when dealing with rabbit/pig models with cardiac penetration holes. Chen et al. [5] used GelMA/oxidized dextran (OD)/borax to construct a high-strength hydrogel network with a triple cross-linked structure, combining photoinitiated polymerized Schiff base bonds with dynamic borate bonds, to effectively adhere to wounds and withstand blood flow pressures. Liu et al. [6] opted for

* Corresponding author. Institution of Disaster and Emergency Medicine, Tianjin University, Tianjin, 300072, China.

** Corresponding author. Institution of Disaster and Emergency Medicine, Tianjin University, Tianjin, 300072, China.

*** Corresponding author. Institution of Disaster and Emergency Medicine, Tianjin University, Tianjin, 300072, China.

E-mail addresses: housk86@163.com (S. Hou), jie.shi@tju.edu.cn (J. Shi), lvqi@tju.edu.cn (Q. Lv).

adding dihydrocaffeic acid (DHCA) into chitosan/glycerophosphate hydrogel to enhance gelation and stable adhesion at near-body temperature (37 °C) to reduce hemostasis time and blood loss. However, the strong adhesion of hydrogels in clinical use poses a risk of *in vivo* tissue adhesion and potentially leads to postoperative complications such as increased pain or the need for secondary surgical interventions [7]. Therefore, the protective and anti-protein functions of materials during the wound healing process have also garnered significant interest. By forming a physical barrier or preventing fibrin adhesion, these materials can effectively protect the wound, prevent direct contact between the injured area and other body tissues, and continue to provide protection for several days post-hemostasis, ensuring proper wound healing. Our aim is to develop hemostatic/anti-adhesion multifunctional hydrogel materials suitable for emergency rescue, focusing on tissue adhesion during wound healing, while achieving rapid treatment of incompressible bleeding.

Poly(lactic acid) (PLA) is a kind of biodegradable polymer polyester, which has been widely used in tissue engineering due to its good mechanical properties and biocompatibility [8]. PLA can be used in bioengineering scaffolds [9] and absorbable sutures [10]. However, its hydrophobic nature has historically limited its research in the field of hemostatic materials [11]. Zwitterionic polymers containing sulfobetaine, phosphate betaine and carboxybetaine base groups have been used as anti-adhesion surface modifiers for *in vivo* implants due to their unique anti-protein properties [12,13]. Notably, sulfobetaine has a structure similar to human betaine, which has high hydrophilicity and biocompatibility. Moreover, sulfobetaine can be covalently attached to polymer surfaces through processes such as click chemistry, endowing the material with additional antifouling characteristics [14]. Derived from collagen proteolysis, gelatin (Gel) is a mixture of polypeptide molecules composed of a variety of amino acids. Its surface is rich in NH₂ sites, and the chain structure features the unique motif of Arg-Gly-Asp (RGD) on the chain structure, which contribute to enhance tissue adhesion, hemostasis and degradability [15,16].

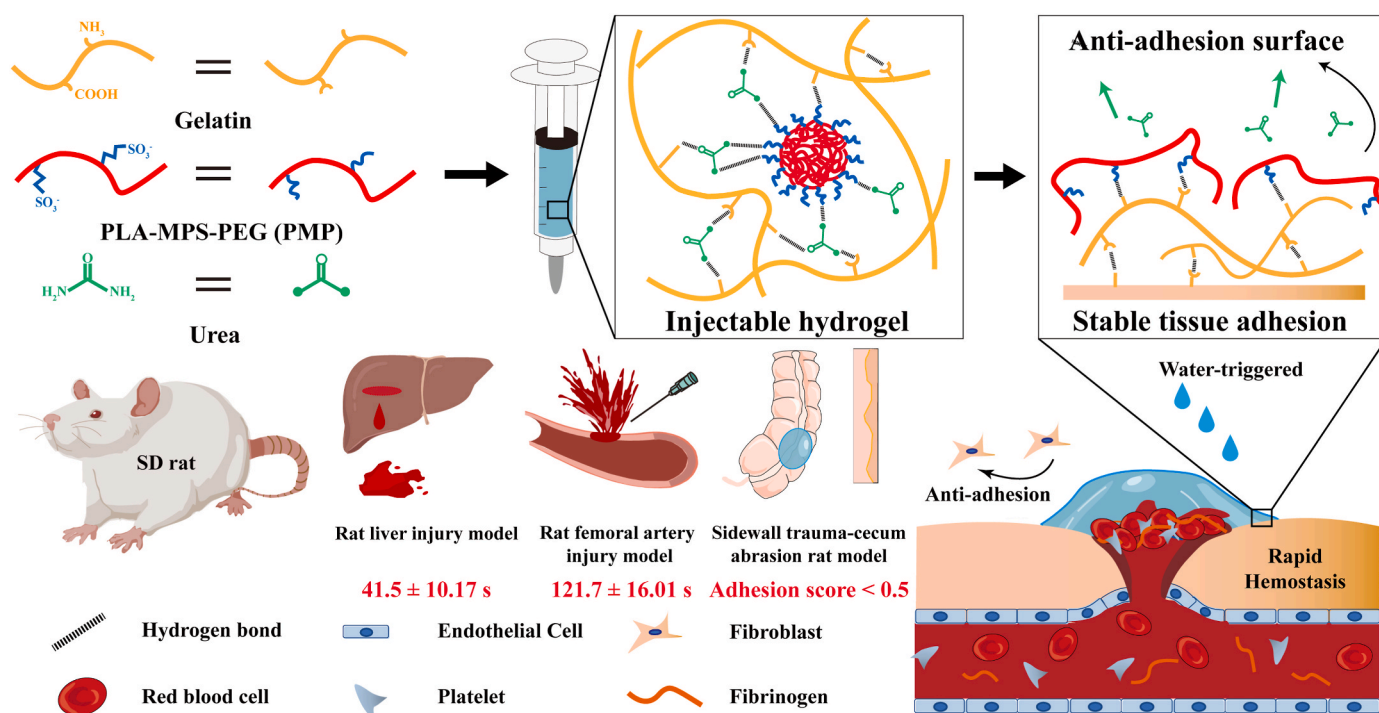
In this work, a small molecule 1-Propanaminium, N, N-bis (2-hydroxyethyl)-N-methyl-3-sulfo-, inner salt (MDEAPS, MPS) was

obtained by sulfonation reaction. Subsequently, PLA-MPS (referred to as PM) was prepared by ring opening polymerization of DL-lactide (LLA) with MPS as initiator. To enhance hydrophilicity, a polyethylene glycol (PEG) segment was incorporated into the polymer chain, yielding PLA-MPS-PEG (referred to as PMP). The injectable hemostatic hydrogel was prepared by blending the polymer with Gel, and its structure was fine-tuned by urea. The incorporation of urea, acting as a hydrogen bond-dissociating agent, modulates the internal cross-linking architecture of the hydrogel [17]. Upon injection into the wound site, water induced spontaneous diffusion of urea molecules from the hydrogel. During the diffusion process, urea dissociates the hydrogen bonds of the original hydrogel, facilitating the disruption and reorganization of PMP micelles, thereby forming an anti-adhesive surface interface on the hydrogel. We hypothesized that the prepared PM-Gel and PMP-Gel hydrogels could effectively cope with incompressible bleeding and prevent subsequent tissue adhesion based on this straightforward and inspiring triggered anti-adhesion system and the anti-protein properties of zwitterions. Following synthesis and characterization, the polymers and hydrogels were further evaluated for their hemostatic and anti-adhesion properties *in vitro*, as well as *in vivo* evaluations of biocompatibility and degradation using rat liver injury and femoral artery injury models (Scheme 1). This research represents an advancement in the application of zwitterionic sulfonate betaine PLA in the realm of biomedical materials, particularly for hemostatic applications.

2. Materials and methods

2.1. Materials

Gelatin from porcine skin (Gel, strength ≥ 250 g bloom, reagent grade) was purchased from Beyotime Biotechnology (Shanghai, China). DL-lactide (LLA, >98.0 % (T)), Urea (>99.5 % (T)), Stannous octanoate (Sn(Oct)₂, 95 %), N-methyldiethanolamine (MDEA, 98 %) and 1,3-propane sultone (1,3-PS, 98 %) were purchased from Aladdin Biological Technology (Shanghai, China). Absorbable Gelatin Sponge was purchased from Xiangen Medical Technology Development Co. LTD.



Scheme 1. Schematic representation of the PMP-Gelatin hydrogel, highlighting its ability to cover irregular wound geometries to form stable adhesion and achieve rapid hemostasis. After water treated, the hydrogel surface undergoes a transformation to a hydrophobic barrier, thereby preventing adhesion.

Commercial hydrogel (mainly composed of carboxymethyl chitosan) was purchased from Saikesaisi Pharmaceutical Technology (Shandong, China).

2.2. Synthesis of PM and PMP

MPS was prepared by the reaction of MDEA with 1,3-PS, and utilized as an initiator for the ring-opening polymerization of lactide to produce betaine-modified polylactic acid (PM). Specifically, 12.0 g lactide and 3.0 g MPS were put into a 100 ml round-bottom flask, vacuumed and circulated N₂ three times, heated in an oil bath to 130 °C, then 0.06 g Sn (Oct)₂ was added with a syringe, and the reaction was heated and stirred continuously for 24 h. PMP was synthesized by adding an additional 1.2 g of PEG to the reaction. After cooling to room temperature, the product was dissolved by adding chloroform, precipitated by cold methanol, and finally a white product was obtained by vacuum drying.

2.3. Preparation of hydrogel

PM or PMP was dissolved in absolute alcohol, Gel or urea was dissolved separately in deionized water by stirring in 60 °C water bath. Then the solutions were mixed and stirred at 60 °C water bath for 90 min to prepare hydrogel, the ratios are shown in Table 1.

2.4. Chemical and physical characterization of material

2.4.1. ¹H NMR

The physicochemical structure of MPS and PMP was verified by proton nuclear magnetic resonance (¹H NMR) spectroscopy (Bruker 400M). Samples of MPS and PMP were dissolved using deuterated water and deuterated dimethyl sulfoxide (DMSO), respectively, with tetramethyl silane (TMS) serving as an internal reference standard.

2.4.2. FT-IR

The structures of Gel, PM, PMP, PLA, and PMP-30 powders were characterized by using a Nicolet 6700 Fourier transform infrared (FT-IR) spectrophotometer (Thermo Scientific). The spectra were acquired in the spectral region of 4000–600 cm⁻¹.

2.4.3. SEM

The surface morphologies of PMP-30 hydrogels were examined by a field emission scanning electron microscope (FE-SEM; Apreo S LoVac, FEI) [18]. Prior to analysis, samples were subjected to freeze-drying, and the surface sections were sputtered with gold.

2.4.4. GPC

The number average molecular weight (M_n) of PMP-30 was tested by Gel Permeation Chromatography system (GPC, TDA305-GPC, Malvern Panalytical). The mobile phase was Tetrahydrofuran (THF) and the mobile phase flow rate was 1 ml/min. Sample concentrations were approximately 0.1 g/ml. The eluent was monitored by a refractive index (RI) detector [19].

2.5. Rheological analysis

The rheological properties of PM-20, PM-30, PMP-20, PMP-30 and

Table 1
The fabricated gels with different PM/PMP/Gel/urea mass ratios.

Sample	Precursor material	Gel (w/v %)	Urea (w/v %)
PM-20	PM	20	10
PM-30	PM	30	10
PMP-20	PMP	20	10
PMP-30	PMP	30	10
PMP-30-U	PMP	30	20

PMP-30-U were evaluated on an MCR 302 rheometer (Anton Paar, Austria) with a 25.0 mm equal plate at 37.0 °C. A liquid collector was employed around the parallel plate to prevent evaporation of water from the gels during testing. *G'* refers to the storage modulus and *G''* refers to the loss modulus, which were measured at a constant frequency of 1 Hz and 1 % strain [20]. The intersection point of *G'* and *G''* was considered indicative of the sol-gel transition [21].

The viscosity of PMP-30 hydrogel was measured under a 1 Hz level with a shear rate of 0.1–100 s⁻¹. The step-strain experiments were performed at 10 % and 200 % strains for regular time intervals, with each phase lasting 60 s, *G'* and *G''* were measured as a function of time.

2.6. Water contact angle test

Cylindrical PMP-30 hydrogels were fabricated within 24-well plates. After water-treated, the hydrogels were maintained at 4 °C for a duration of 24 h. The hydrophilicity of both water-treated and untreated hydrogel surfaces was quantitatively assessed using a contact angle goniometer. Specifically, water contact angles were recorded at various hydrogel surface locations after 30 s after dropping.

2.7. Fluorescence microscope observation

According to Hu's method [22], 5 % TVPA (a water-soluble luminogen with aggregation-induced emission) was added to the PMP-30 hydrogel. The surface morphology of the hydrogel was observed under an inverted fluorescence microscope (Nikon Eclipse Ts2). The morphology of the hydrogel surface was observed and recorded before and after water treatment.

2.8. Swelling kinetics evaluation

The swelling behavior of PM-30 and PMP-30 was tested using Li's method [23]. 0.3 ml of PM-30 or PMP-30 hydrogel was injected into the 24-well plate to form cylindrical shape, then the hydrogels were immersed in PBS solution (PH 7.4) followed by incubation at 37 °C. At each time point, the swelling hydrogels were taken out and weighed. The swelling ratio was evaluated using the following formula:

$$\text{swelling ratio (\%)} = \frac{W_t - W_0}{W_0} \times 100$$

where *W_t* is the hydrogel weight at the specific time and *W₀* is its weight at *t* = 0.

2.9. Tissue adhesion test

The adhesive properties of PMP-30 in wet conditions were assessed using fresh porcine skin tissues. 0.3 ml of PMP-30 was applied to the surface of the porcine skin, followed by spraying deionized water onto the hydrogel surface. Subsequently, the adhesion stability of PMP-30 was determined by bending, folding, or continuously observing pigskin placed under flowing water.

In order to evaluate the adhesion strength of the hydrogels on biological tissues, lap shear tests were conducted utilizing a tensile testing machine. The PMP-30 hydrogel was injected between two pieces of porcine skin tissue, with a contact area measuring 15 mm × 15 mm. These two pieces of skin tissue were then placed on the tensile testing machine and stretched in one direction at a rate of 5.0 mm/min until detachment occurred between them.

2.10. Cytocompatibility testing

The cytocompatibility of PMP-30 was assessed using the leaching solution method with L929 mouse fibroblasts or human umbilical vein endothelial cells (HUVECs) [24]. Cell counting kit-8 (CCK-8) and

live/dead (viability/cytotoxicity kit) assays were used to evaluate the growth status of cells, respectively.

For CCK-8 assays, after conventional cell culture, cells were seeded in 96-well tissue culture plates and cultured using 200 μ l of the PMP-30 solutions (0.1 mg/ml freeze-dried PMP-30 in culture medium for 24 h), continuously incubating at 37 °C with 5 % CO₂. The culture medium (RPMI 1640 with 10 % FBS and 1 % penicillin/streptomycin) was changed every 2 days. At 1, 3 and 5 days, the proliferation rate of L929 cells was tested by a CCK-8 assays. The absorbance of the culture medium was measured using an enzyme marker at 450 nm. Cell viability was measured using the following equation:

$$\text{cell viability (\%)} = \frac{A_t}{A_c} \times 100$$

where A_t and A_c are the absorbance of the supernatants of the PMP-30 and control groups, respectively.

For the live-dead staining assay, the culture medium was removed from the well plate at 1, 3, and 5 days. The cells were then stained with calcein-AM and propidium iodide (PI) to observe cell morphology using an inverted fluorescence microscope (Nikon Eclipse Ts2) [25]. Live cells (calcein-AM-stained green) were distinguished from dead cells using PI stained.

2.11. Hemolytic activity test

The anticoagulated rat blood was diluted in PBS and centrifuged at 1500 rpm for 5 min. The experiment was repeated three times to obtain a 10 % erythrocyte suspension in PBS. Subsequently, 500 μ l of the erythrocyte suspension and 500 μ l of hydrogels were combined and coincubated at 37 °C for 1 h. After centrifugation at 2500 rpm for 5 min, the absorbance of the supernatant was measured at 540 nm. In addition, PBS was selected as the negative control group, and Triton X-100 was selected as the positive control group. The hemolysis rate was measured using the following formula:

$$\text{hemolysis rate} = \frac{A_s - A_n}{A_p - A_n} \times 100$$

where A_s , A_p , and A_n are the absorbances of the PM/PMP hydrogels, positive control and negative control, respectively.

2.12. In vitro anti-adhesion

The cell adhesion property of PMP-30 was assessed by coincubation with L929 cells. The specific operation was strictly based on methods provided by Wei et al. [26].

2.13. In vitro degradation

The weight remaining ratio was used to evaluate PMP-30 degradation behavior *in vitro*. The experimental scheme is adapted from our previous method [7]. 0.3 ml of PM-30 or PMP-30 hydrogel was injected into the 24-well plate to form cylindrical shape, then the hydrogels were immersed in PBS solution (PH 7.4) followed by incubation at 37 °C. The weight remaining ratio (%) was measured using the following formula:

$$\text{weight remaining ratio (\%)} = \frac{W_1}{W_0} \times 100$$

where W_0 is the initial dry weight of hydrogel and W_1 is the post-degradation weight of the hydrogel, respectively.

2.14. In vitro hemocompatibility evaluations

The *in vitro* whole blood clotting test and tube inversion method were used to investigate the hemostasis effect of PM and PMP hydrogels [27, 28]. The experiments were performed with reference to the cited

literature, and the blood clotting index (BCI) was measured using the following formula:

$$\text{BCI (\%)} = \frac{I_s - I_o}{I_B - I_o} \times 100$$

where I_s , I_B , and I_o are the absorbance of the PM/PMP hydrogel group, control group, and blank well, respectively.

2.15. Animal experiments

All animal experiments were conducted by the Guidelines for the Care and animal protocols were approved by the Institutional Animal Care and Use Committee of Yi Shengyuan Gene Technology (Tianjin) Co., Ltd. (protocol number YSY-DWLL-2024428, GENINK-20230004). Male Sprague Dawley rats (220–250 g) were purchased from Beijing HFK Bioscience Co., Ltd. (Beijing; SCXK 2019-0008).

2.15.1. In vivo anti-adhesion

The sidewall trauma-cecum abrasion rat model was chosen to validate the anti-adhesion performance of PMP-30 hydrogel [29]. Male Sprague Dawley rats (SD rats) were randomly divided into three groups ($n = 6$), after being anesthetized, the peritoneum was opened by a 5 cm long incision along the linea alba on the abdominal wall. Following the previous method, a cecal trauma model was established with some modifications. The cecal serosa was bluntly separated and damaged using forceps to cause bleeding without perforation. Similar damage was also created on the opposite side of the abdominal wall from the cecal using forceps. For the PMP group, 0.3 ml of PMP-30 was injected into the injured cecum wound surface, followed by spraying deionized water onto the hydrogel surface. Similarly, 0.3 ml of commercial hydrogel was injected into the wound site in the same manner for the control group. At 14 days after modeling, the rats were sacrificed and the abdominal cavity was opened to observe postoperative adhesion. A standard adhesion scoring system was used for blinded assessment of adhesion severity, with scores ranging from 0 to 5 [30]. Tissue specimens from the damaged area of the cecum and adjacent tissues adhered to the cecum and abdominal wall were collected for histopathological examination, including H&E and Masson's trichrome staining.

2.15.2. Degradation and biocompatibility in vivo

In vivo degradation and biocompatibility of PMP-30 were assessed by subcutaneously implanting the hydrogel into the dorsal tissue of male SD rats [31]. 0.5 ml of PMP-30 was first modeled into a cylindrical shape at 4 °C and then soaked in deionized water before being implanted. After anesthetization, the cylindrical PMP-30 was placed into the rat's dorsal subcutaneous tissue. At day 3, 7, and 14, one rat was executed for post-implantation evaluation. Additionally, H&E and Masson trichrome staining were performed on the surgical site tissue to assess degradation behavior.

2.15.3. Rat liver injury model

Rat liver injury model was conducted using the method provided by Chen et al. [32] After modeling and allowing for 5 s bleeding, PMP-30 hydrogel was injected onto the bleeding site and then sprayed with deionized water on the surface. Commercial gauze or gelatin sponge (GS) was applied on the bleeding site as control group. Bleeding volume and hemostasis time were measured. All rats were sacrificed to examine postoperative healing and whether there was adhesion *in vivo* at 7 days after successful modeling. In addition, tissue specimens from the injured livers were collected for histopathological examination, including H&E and Masson's trichrome staining.

2.15.4. Measurement of coagulation parameters

Coagulation parameters, including the values of activated partial thromboplastin time (APTT), prothrombin time (PT), thrombin time

(TT), and fibrinogen (FIB), were measured using an automatic coagulation analyzer. The experiment was conducted according to the method Section 2.15.3. One hour after the modeling, blood was collected from the abdominal aorta of rats using tubes containing sodium citrate as an anticoagulant. The samples were centrifuged at 3000 rpm for 15 min to obtain the test plasma [33].

2.15.5. Rat femoral artery injury model

After Male SD rats were anesthetized, the skin of the inner limb of the

hind leg was incised to expose the femoral artery, which was stripped from the femoral vein. A 26 G needle syringe was utilized to injure the artery without complete disconnection, and a 5-s period of bleeding was permitted to ensure normal blood loss. Then, 0.5 ml of PMP-30 was injected onto the bleeding site, and the hemostasis time was recorded.

2.16. Statistical analysis

statistical analysis was determined using one-way analysis of

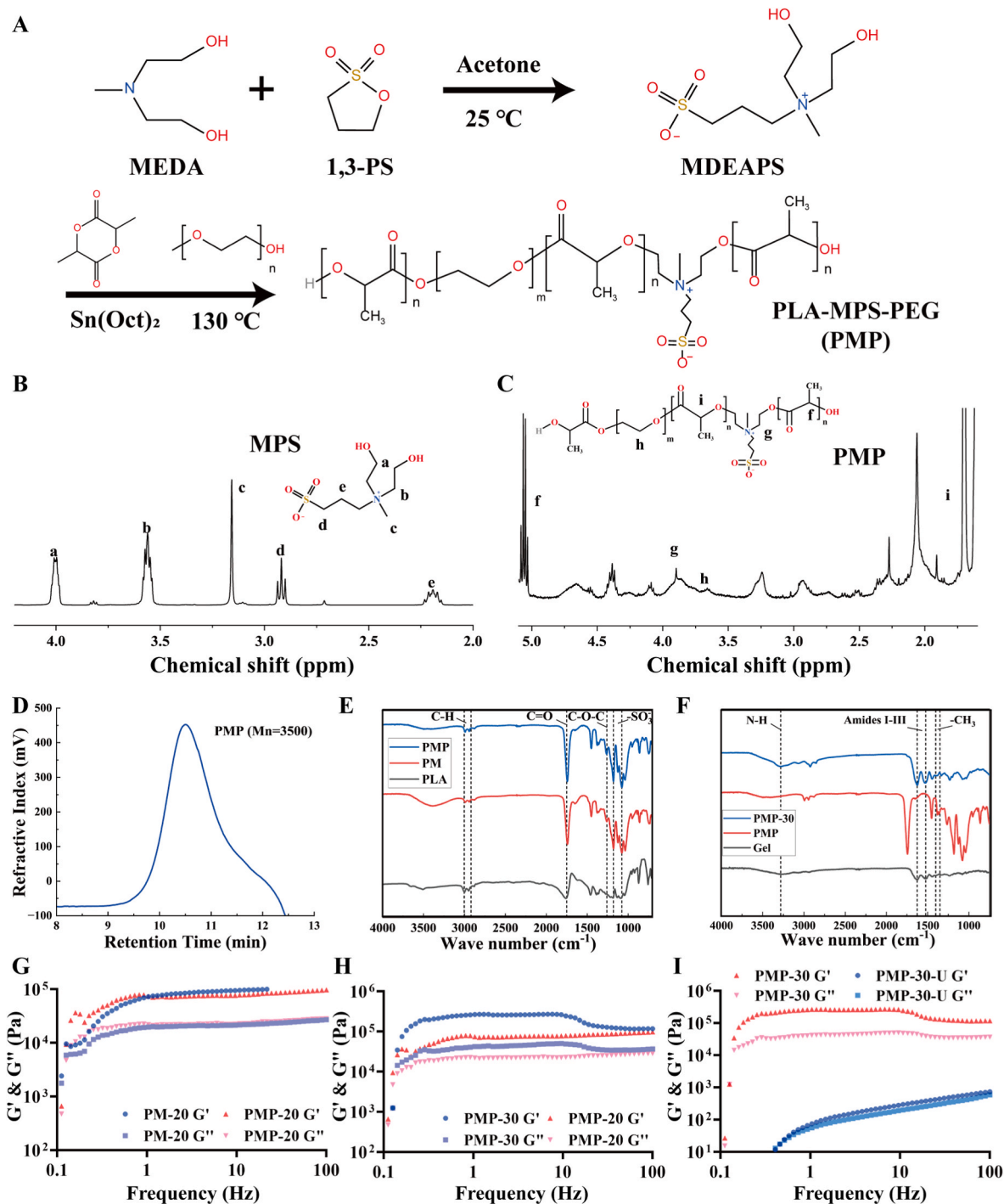


Fig. 1. Physicochemical, morphological, and rheological characterizations of PMP and PM developed from MPS, PEG and LLA. (A) Synthesis of PMP. (B) $^1\text{H NMR}$ spectra of MPS. (C) $^1\text{H NMR}$ spectra of PMP. (D) GPC spectra of PMP ($M_n = 3500$). (E) FTIR spectra of PLA, PM and PMP. (F) FTIR spectra of Gel, PMP and PMP-30. (G) Rheological properties of PM-20 and PMP-20 at 37 °C. (H) Rheological properties of PMP-20 and PMP-30 at 37 °C. (I) Rheological properties of PMP-30 and PMP-30-U at 37 °C.

variance (ANOVA) followed by GraphPad Prism and Origin 8.0 software. The results are expressed as the mean \pm the standard deviation (SD). In all cases, differences were considered significant if $P < 0.05$.

3. Results and discussion

3.1. Synthesis of PM and PMP

Herein, MPS was first generated by the sulfonation reaction of MDEA and 1,3-PS. Next, betaine modified PLA named PM and PMP were prepared by using MPS as initiator to promote the ring opening reaction of lactide and introducing zwitterionic groups into the structure of PLA (Fig. 1A). In the ^1H NMR spectrum of MPS (Fig. 1B), a peak at 4.02 ppm represented the proton peak of $-\text{CH}_2\text{OH}$ -, b peak at 3.55 ppm represented the proton peak of $-(\text{CH}_2)_3\text{N}^+$ -, c peak at 3.16 ppm represented the proton peak of the methyl group on the nitrogen atom. D peak at 2.92 ppm and the e peak at 2.19 ppm represented the two proton peaks of the sulfonate group. The results of ^1H NMR spectra indicated the successful synthesis of MPS. In the ^1H NMR spectrum of PMP (Fig. 1C), f peak at 5.06 ppm and i peak from 1.40 to 1.70 ppm showed the proton peak of methyl and methylene groups in the PLA polymer chain. G peak at 3.89 ppm represented the proton peak of $-(\text{CH}_2)_3\text{N}^+$ -, which confirmed that MPS was grafted into PLA. H peak at 3.66 ppm represented the proton peak of $-\text{CH}_2-$, indicating the integration of PEG and the successful synthesis of PMP. In Fig. 1D, the results of GPC gel chromatography showed that the synthesized PMP was relatively monodisperse, and the number average molecular weight (Mn) was about 3500.

3.2. Synthesis and characterization of hydrogels

A series of PM or PMP hydrogels were prepared to maintain a flowing sol state at human body temperature and to exhibit a membrane-like structure upon water treatment. The interaction among Gel and PM/PMP in the hydrogel was confirmed by FTIR. As shown in the FTIR spectrum of Fig. 1E, the absorb peak between 2900 and 3000 cm^{-1} belonged to the C-H stretching vibration, and the absorption peak at 1756 cm^{-1} belonged to the C=O stretching vibration, confirming the existence of ester groups, and the peak at 1382 cm^{-1} belonged to the characteristic peak of methyl group, these peaks confirmed the structure of polylactic acid [34]. Due to the introduction of PEG, the FTIR of PMP has a more obvious peak at 1260 cm^{-1} , representing the stretching vibration of C-O-C [14]. The absorption peaks of 1190 and 1075 cm^{-1} appeared in PM and PMP were the main characteristic peaks of sulfonate group, which proved that sulfobetaine was successfully synthesized into the structure of PLA. In Fig. 1F, the band around 3287 cm^{-1} represents the N-H vibration derived from gelatin amine groups, and the peak at 1622 and 1527 cm^{-1} was the amide I-III absorption band, which showed the conformational sensitive band of polypeptide and protein. The shift and broadening of the N-H vibration region also demonstrate the formation of intermolecular hydrogen bonds between Gel and PM/PMP. The absorption peak changes in PMP hydrogel were similar to those in PM hydrogel indicating that grafting PEG did not affect cross-linking within the hydrogel. During the synthesis of PMP, the integration of the PEG segment into the PLA main chain meant that no additional groups were present to react with Gel.

Subsequently, the gelation dynamics of the hydrogel were measured by evaluating the energy storage modulus (G') and loss modulus (G'') of the material by dynamically scanning in the frequency range from 0.1 to 100Hz (Fig. 1G–I). For all hydrogels evaluated, G' consistently exceeded G'' , signifying a solid-like gel state at physiological temperature (approximately 37 °C). The increase of gelatin content enhanced the rheological properties of the hydrogel, whereas the incorporation of PEG in the precursor material had little effect. This may be attributed to the fact that MPS serves as the main crosslinking site for this material, and therefore, introduction of PEG into the chain has little impact on its overall rheological properties. To further elucidate this, we standardized

the gelatin concentration at 30 % and fabricated a series of hydrogels with varying urea concentrations to assess their state at 37 °C for potential solidification (Fig. S1). It was observed that when the urea ratio was set at 20 %, fluidity of the hydrogel was maintained; however, rheological measurements showed a significant decrease in both G' and G'' , resulting in a crossing point which indicated loss of gelation properties. Consequently, this specific ratio was deemed inappropriate for practical applications due to its compromised mechanical integrity.

The microstructure of the hydrogel material was examined through SEM. As shown in Fig. 2A, the microstructure of PMP-30 hydrogel showed uniform and porous structure. Notably, after water was sprayed on the hydrogel surface, a smooth membrane-like structure was observed, which is conducive to its subsequent anti-adhesion property. To substantiate the morphological alterations on the hydrogel surface pre- and post-water treatment, a water contact angle test was performed. The water contact angle on the surface of PMP-30 hydrogel pretreated with water was significantly higher compared to the untreated hydrogel, it was found that the water contact angle increased from about 28° to about 70° (Fig. 2B, C, E). This enhancement in hydrophobicity post water treatment indicates a significant change in the hydrogel's surface morphology.

To further discuss the chain structural changes and the hydrophobic transition on the hydrogel surface, we incorporated TVPA, the aggregation-induced emission luminogens (AIEgens) into the hydrogel, which serves as a fluorescent probe responsive to the hydrophilic-hydrophobic transition of the hydrogel. As shown in Fig. 2D, slowly adjust the focal length of the fluorescence microscope to emphasize the observation of the surface morphology of the hydrogel before and after water treatment. The appearance of various colored Newton's rings on the hydrogel surface represents the superposition of light interference generated by different surface morphologies. These irregular combinations are formed by the inconsistent refractive index between aggregated PMP micelles and highly hydrated gelatin regions. After water treatment, the PMP polymer domains expanded and predominated, covering the hydrogel surface, indicating the disruption and migration of PMP micelles. The surface of the hydrogel was further observed under red fluorescence at 610 nm, only a small amount of TVPA was observed at the initial state of the PMP-30 hydrogel. However, after water treatment, a substantial amount of TVPA was evident on the hydrogel surface. The polar aggregation luminescence and corresponding characteristics of TVPA visualize self-enhancement behavior in PMP hydrogels. After water treatment, urea molecule transfer promotes destruction and transfer of PMP micelles from aggregate structures, exposing more hydrophobic groups. The connection of micelles on the hydrogel surface increased its hydrophobicity and finally formed an anti-adhesion film structure.

As a small molecule hydrogen bond dissociation/generation agent, urea can be incorporated into hydrogels to disrupt and fill more hydrogen-bonded structures [35,36]. This process reduces the mechanical strength of the hydrogel and transforms it into an injectable form. However, high concentration of urea will reduce the modulus of the hydrogel and make it difficult to perform sol-gel transition (Fig. 1I). In the PMP-Gel hydrogel, PMP segments exist in the form of micelles, and the hydrophilic zwitterionic sulfobetaine segments can form hydrogen bond interactions with gelatin or urea, which enables the hydrogel to be injectable. After water treatment, urea diffusion induces the dissociation of the hydrogel's hydrogen bonds, enabling the disruption and reorganization of PMP micelles, thereby forming an anti-adhesive interface. Moreover, hydrophilic end groups exposed through hydrogen bond dissociation in both gelatin and PMP can establish new cooperative bonds with adhesive surface groups, enhancing the hydrogel's adhesiveness. Consequently, the hydrogel develops a dual-sided Janus structure that is anti-adhesive on the exterior and promotes adhesion on the interior [17]. As shown in Fig. S3, after a brief treatment of deionized water to the surface and subsequent water removal, an anti-adhesion film was formed on the surface of the

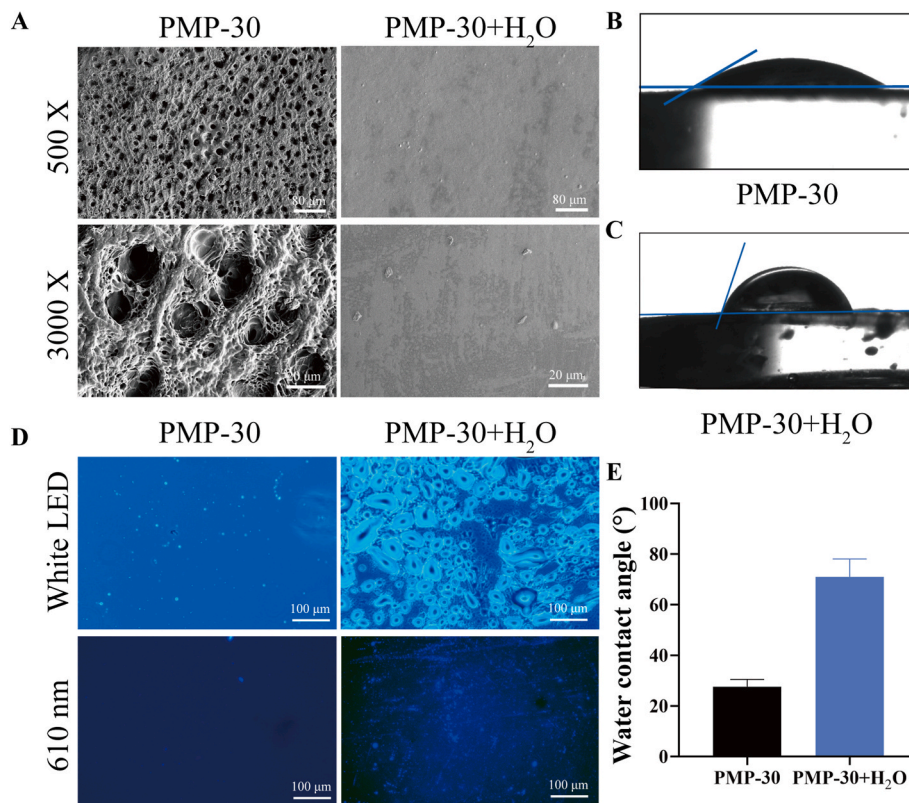


Fig. 2. (A) SEM images of PMP-30 and water-treated PMP-30 (PMP-30+H₂O). Water contact angle of (B) PMP-30, (C) PMP-30+H₂O. (D) Fluorescent microscopy visualization of PMP-30 and PMP-30+H₂O. (E) Water contact angle comparison. Data indicate the mean \pm SD (n = 3).

PMP-30 hydrogel so that adhesion could not be generated. In contrast, treatment of a saturated urea solution for the same duration left the PMP-30 hydrogel in a viscous state. Furthermore, the structure of the urea-free PMP-30 hydrogel was compromised due to rapid swelling in both deionized and saturated urea solutions.

3.3. Injectability and tissue adhesive tests

The gelation time of the PMP-30 hydrogel was tested at 37 °C, as shown in Fig. 3A, with the PMP-30 exhibiting a gelation time of approximately 80 s. The thermosensitivity of gelatin can influence the gelation time of the hydrogel, and for patients with blood loss, a further decrease in body temperature may result in a reduced gelation time. The PMP-30 hydrogel demonstrated non-Newtonian shear thinning (pseudoplastic) behavior in both strain sweep tests and viscosity tests. As shown in Fig. 3B, with the gradual increase in shear strain to a critical point, the storage modulus (G') of the hydrogel rapidly decreased below the loss modulus (G''), indicating a transition from a gel to a sol state. As illustrated in Fig. 3C, the viscosity of the hydrogel progressively decreased with increasing shear rate. Additionally, the self-recovery capability of the PMP-30 hydrogel was assessed using dynamic cyclic strain sweep measurements. Oscillating strains of 10 % and 200 % were applied in alternating phases (Fig. 3D). At a strain of 200 %, the storage modulus (G') rapidly diminished, falling below the loss modulus (G''), signifying the temporary structural breakdown of the hydrogel. Upon returning the strain to 10 %, G' swiftly rebounded to a level near its initial value, indicating rapid hydrogel reconstruction facilitated by reversible hydrogen bonding. Even after three cycles of alternating 10%–200 % strains, the PMP-30 hydrogel reliably reverted to its original gel state.

As previously discussed, the structure of the hydrogel enables it to be injectable, allowing it to extrude from the needle of a 1 ml syringe and form the desired shape (Fig. 3E). This characteristic could fulfill the

requirements of minimally invasive surgery and management of incompressible bleeding. To demonstrate its self-healing ability, one disk-shaped hydrogel was bisected, half was stained with methyl orange solution, and the two pieces were placed in edge contact. The hydrogel tightly bonded within 1 h and uniformly fused in color (Fig. 3F).

After injection of into porcine skin pieces, the hydrogel remained firmly attached without detachment following repeated stretching, bending, and water rinsing (Fig. 3G and H), indicating robust and stable tissue adhesion strength. The lap shear strength of the hydrogel on pig skin pieces was tested according to the previous method, and the load-displacement curve was plotted from the test data (Fig. 3I). The lap shear strength of the hydrogel was 40.8 kPa, surpassing that of fibrin glue (approximately 10 kPa) and other gelatin-based hemostatic agents [37]. The adhesion between the hydrogel and tissues is primarily due to the unique binding sites of gelatin and the multitude of hydrogen bonds formed with tissue proteins. After the diffusion of small molecule urea from the hydrogel and the subsequent migration of PMP micelle, more hydrophilic end groups are exposed, further enhancing hydrogel-tissue adhesion [17].

3.4. Hemocompatibility test

For biomaterials used *in vivo*, especially those that come into contact with blood, biocompatibility must be rigorously evaluated to ensure no adverse effects on human health. Herein, the blood compatibility and cell compatibility of PMP hydrogels were tested. The hemolytic activity of the hydrogel was first characterized using a rat red blood cell suspension in contact with the hydrogel. After incubation at 37 °C for 1 h, the hemolysis rate was less than 5 % in every hydrogel group (Fig. 4A and B), which met the requirements set by the American Society of Testing Materials.

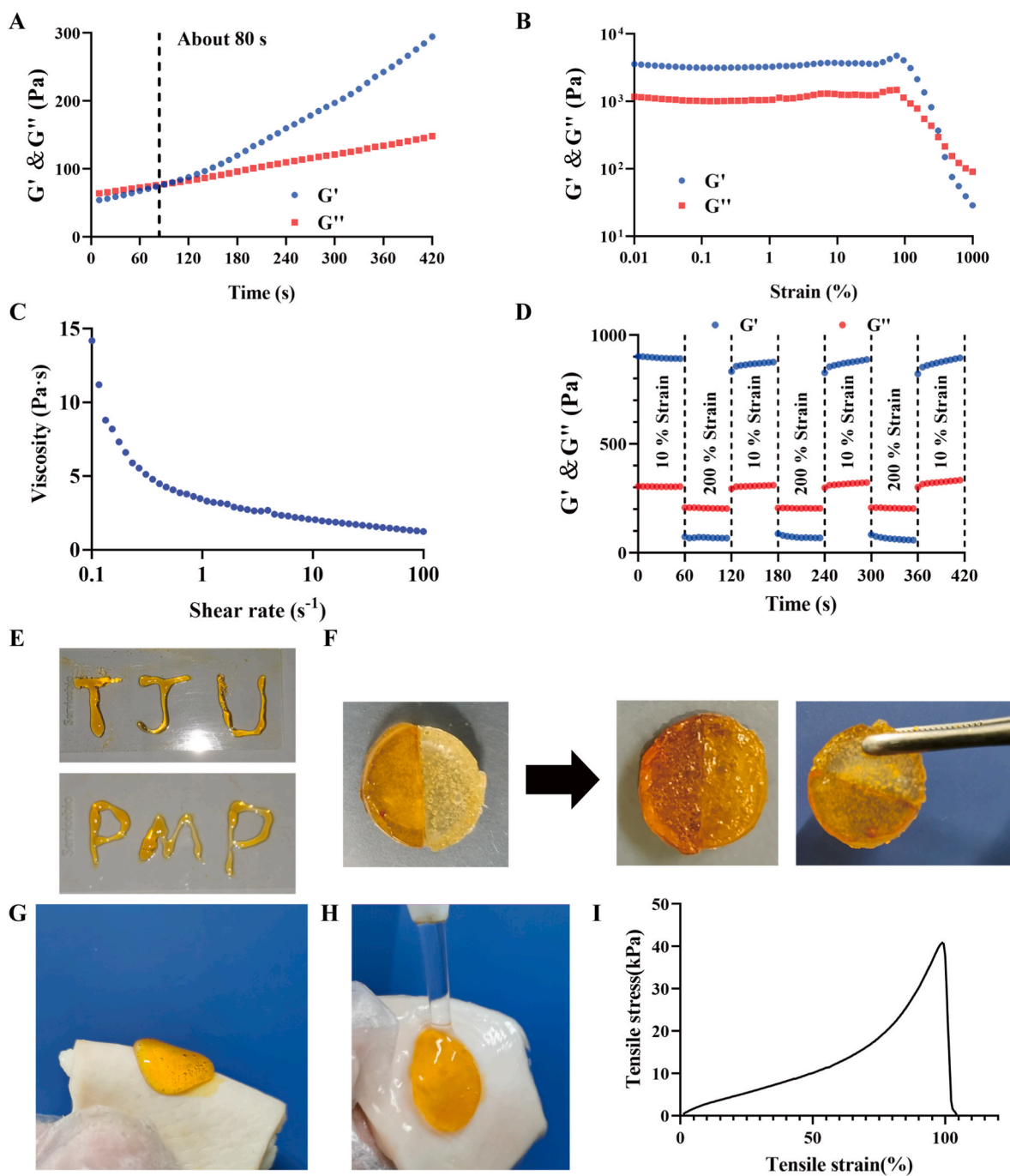


Fig. 3. Injectability and tissue adhesive tests of hydrogel. (A) Gelation time of PMP-30. (B) Strain sweep test of PMP-30. (C) Viscosity measurement of PMP-30. (D) Dynamic cyclic strain sweep measurement of PMP-30, ($\omega = 4$ rad/s, $\gamma = 10$ or 200 %, $t = 37$ °C). (E) Injectability of PMP-30. (F) Self-recovery ability of PMP-30. (G) Tissue adhesive test of PMP-30 under dry conditions. (H) Tissue adhesive test of PMP-30 under flowing water. (I) Stress-strain profile of PMP-30.

3.5. *In vitro* cell culture

CCK-8 and live/dead assays were used to evaluate cytocompatibility of PMP-30 hydrogel. Herein, L929 fibroblasts and human umbilical vein endothelial cells HUVECs were used as the subjects of the experiment. After 1, 3, and 5 days of incubation in the medium containing the hydrogel leaching solutions, the cells showed comparable cell viability to that of the control group. Notably, on the 5th day, HUVECs cocultured with the extract displayed significantly higher cell viability ($P < 0.05$), while cell viability at other time points was not significantly different from the control group (Fig. 4C and D). Live/dead staining results revealed that both cell types exhibited normal growth, presenting

a green, spindle-like morphology under fluorescence microscope, with minimal red-stained dead cells observed (Fig. 4E and F).

The outstanding biocompatibility of PMP hydrogel can be attributed to the use of human-friendly raw materials. PLA and Gel have been well-documented as non-toxic to humans [38], and polymers containing PEG or sulfobetaine groups have been successfully applied in healthcare and related fields [39,40]. Consequently, this type of hydrogel holds great promise for development in hemostatic materials research.

3.6. Swelling and degradation properties

The administration of hydrogels via injection may potentially induce

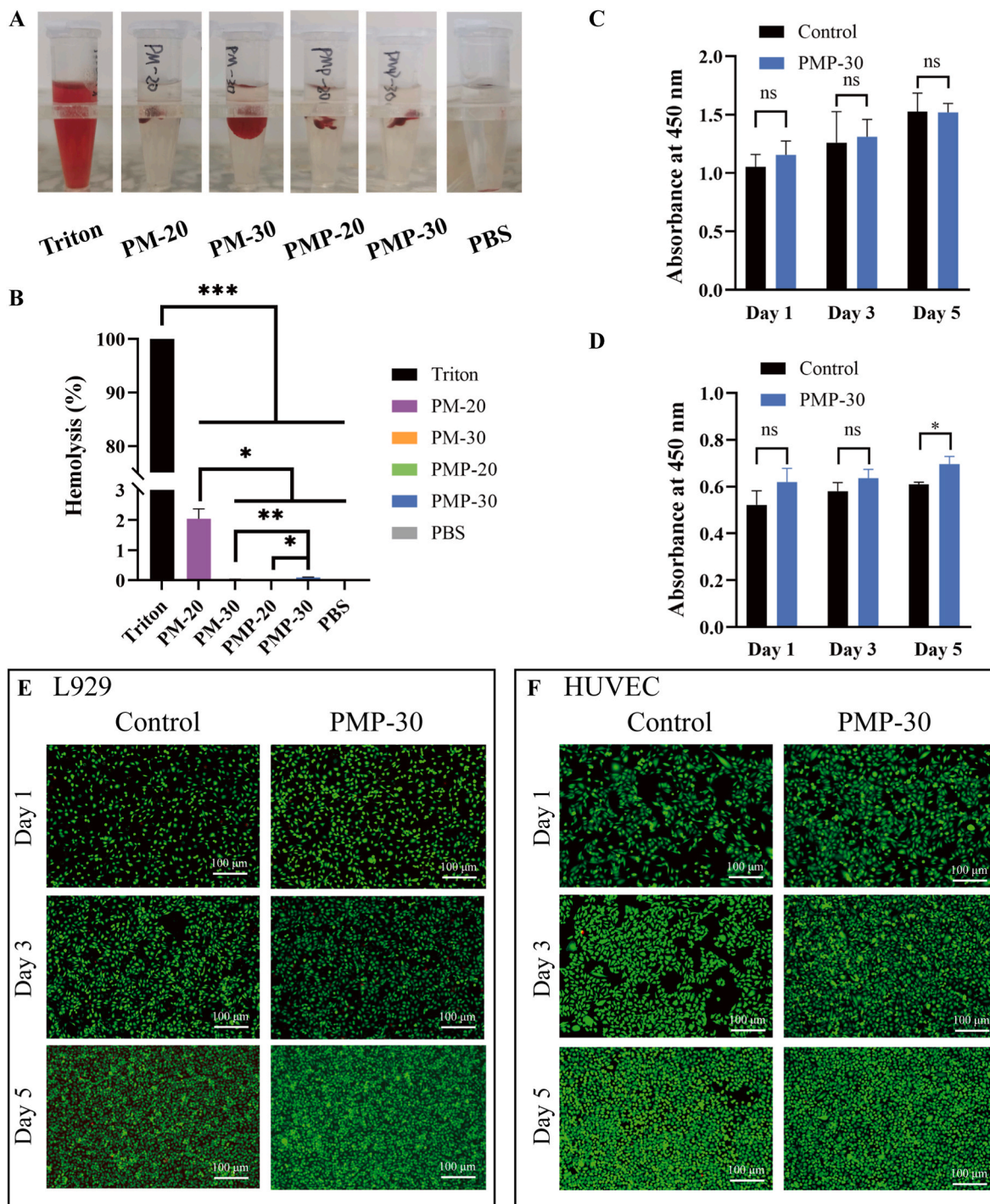


Fig. 4. Hemolytic activity and cytocompatibility testing of PM and PMP hydrogels. (A) Image and (B) hemolysis rates of hydrogels. (C) L929 cell viability when in contact with PMP-30 leaching solution. Data are presented as the mean \pm SD (n = 6). (D) HUVEC viability when in contact with PMP-30 leaching solution. Data are presented as the mean \pm SD (n = 6). (E) Live/dead staining of L929 cells after contact with PMP-30 leaching solution and nutrient solution for 1, 3, and 5 days. (F) Live/dead staining of HUVECs after contact with PMP-30 leaching solution for 1, 3, and 5 days.

tissue inflammation or allergic responses in the surrounding tissues. Hydrogels are capable of absorbing bio-fluids around the wound. However, it is important to consider that swelling and volume expansion of hydrogels may lead to compression of adjacent tissues. Additionally, high water content can also lead to rapid degradation of hydrogels. In addition, the degradation products should have no additional toxicity risk [41]. We hope that hydrogels will not lead to additional adverse effects during injection and degradation processes. *In vitro* degradation experiments of the hydrogel were performed in phosphate-buffered

saline (PBS, pH = 7.4), and the volume of the hydrogel was reduced by about 76 % after incubation at 37 °C for 72 h (Fig. S2). Due to the higher cross-linking density, the average swelling ratio of PM-30 and PMP-30 hydrogels is both less than 30 %. In the subcutaneous implantation experiments, the water-treated PMP-30 hydrogel discs degraded progressively in rats over time. As shown in Fig. 5, the implanted hydrogel completely degraded within 7 days, with no noticeable redness or swelling in the surrounding tissue. Histopathological changes were assessed by H&E and Masson trichrome staining. The material did not

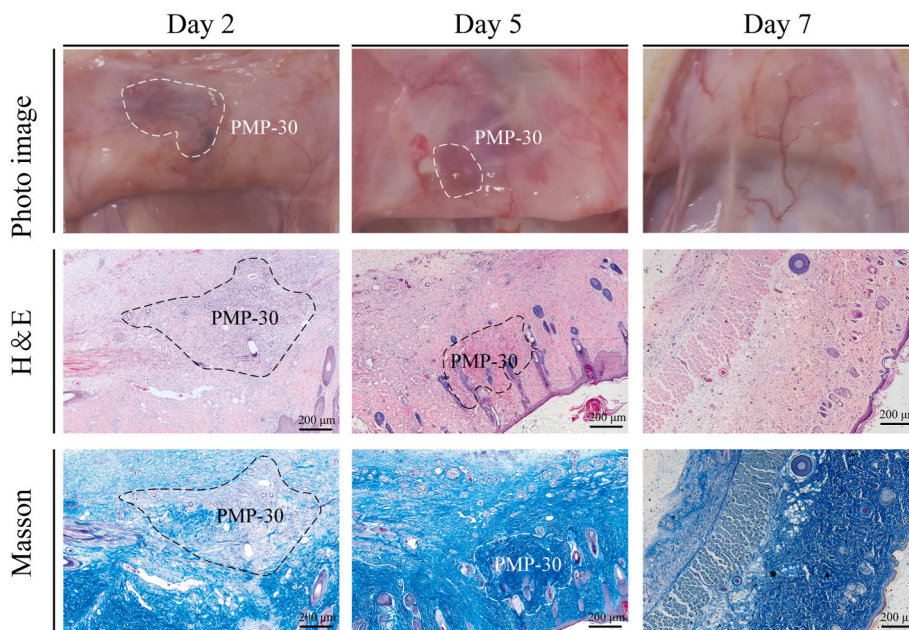


Fig. 5. Gross images, H&E and Masson trichrome staining of implanted PMP-30 hydrogel in the rat dorsal subcutaneous tissue. The region contained by the dashed line represents the remaining PMP-30 hydrogel.

cause obvious inflammation during degradation. A minimal presence of neutrophils was observed around the material remnants in the stained sections. As the material degraded, the presence of neutrophils gradually decreased while collagen production increased. By day 7, no material remnants were visible under the naked eye, and the inflammatory response had subsided in the stained sections. These results confirmed that the implantation of the PMP-30 hydrogel *in vivo* does not cause adverse effects on the tissue and the degradation byproducts do not inflict additional harm.

3.7. Anti-adhesion properties

PMP-30 hydrogel can prevent tissue adhesion through the formation of a smooth anti-adhesion surface formed after water treatment and the anti-protein property of betaine sulfonate. *In vitro* anti-adhesion experiments, the PMP-30 hydrogel was treated with deionized water, introduced into the culture medium, and co-cultured with L929 fibroblasts for a duration of 24 h to monitor cell adhesion and proliferation. As shown in Fig. 6A, L929 fibroblasts in the control group adhered typically and covered the culture dish and maintained a firm attachment even post PBS rinsing. Conversely, no cell adhesion was observed on the surface of the PMP-30 hydrogel, and only a few cells suspended in the medium. These results indicate that the unique membranogenicity and anti-protein effects of PMP-30 can effectively prevent fibroblast adhesion proliferation and avoid postoperative adhesion problems.

The sidewall trauma cecum abrasion rat model was utilized to assess the *in vivo* anti-adhesion performance of PMP-30 hydrogel, as previously reported [7]. Both commercial hydrogel and PMP-30 significantly mitigated the extent of adhesion (Fig. 6B, $P < 0.01$ compared with the model group). The commercial hydrogel group showed multiple minor adhesions (Fig. 6C), potentially attributable to incomplete coverage at the abrasion site by the injected hydrogel or its displacement to other body regions, leading to an increasing risk for subsequent adhesion issues. Conversely, there was almost no adhesion observed in PMP-30 hydrogel group; culminating in reduced overall adhesive scores. The cecum could be separated from the abdominal cavity freely, with no adverse tissue damage was observed at the abrasion site. H&E staining of the model group revealed a proliferation of inflammatory cells, and Masson trichrome staining indicated substantial fibrin deposition,

leading to adhesion between the abdominal wall and the cecum. The same inflammatory cell aggregation occurred in the H&E staining of the commercial hydrogel group, along with observed adhesion. In contrast, the PMP-30 hydrogel group presented with reduced inflammatory cell infiltration and minimal residual material in H&E staining, owing to its biodegradability. No significant fibrin deposition was observed in Masson trichrome staining. Even when the PMP-30 hydrogel was almost completely degraded, there was still no adhesion at the damaged tissues. These results demonstrate that PMP-30 hydrogel possesses superior anti-adhesion properties, where the water-based polymeric anti-adhesion membrane (early time) and sulfobetaine anti-protein effect (over time) act in concert to facilitate wound healing.

3.8. *In vitro* hemostasis test

Whole blood coagulation time (BCT), coagulation inversion test and blood clotting index (BCI) experiments were used to evaluate the hemostasis effect of hydrogel *in vitro*. It was observed that coagulation did not occur until the gauze was incubated with whole blood for about 180 s, whereas in the control group, the blood remained flowing for over 200 s. The BCT of PM and PMP hydrogels was similar to that of commercial gelatin sponges, with the fastest time was about 80 s to form completely stable, self-supporting gel (Fig. 7A and B). In the subsequent coagulation inversion experiment, the EP tube was inverted every 15 s following the introduction of whole blood in each group, and the PMP-30 hydrogel could coagulate blood in 45 s without shedding (Fig. 7C). BCI quantifies the coagulation velocity of the material, a higher BCI indicates a slower coagulation rate [42]. The PMP-30 group had obvious clot adsorption within 30 s, and the BCI value was lower than that of other groups (Fig. 7D). Furthermore, it was observed that the hemostatic performance of hydrogels was influenced by the Gel content. After blood absorption through the hydrogel's porous structure, the electrostatic interactions between Gel, the zwitterionic and plasma components facilitate blood coagulation. The results also indicated that PMP hydrogel with improved hydrophilicity showed superior hemostatic effect compared to the PM hydrogels, which may be due to the less hydrophobic interface. The results of *in vitro* hemostasis test showed that PMP-30 had better hemostatic effect than other groups of hydrogels, so the PMP-30 hydrogel was selected for subsequent animal

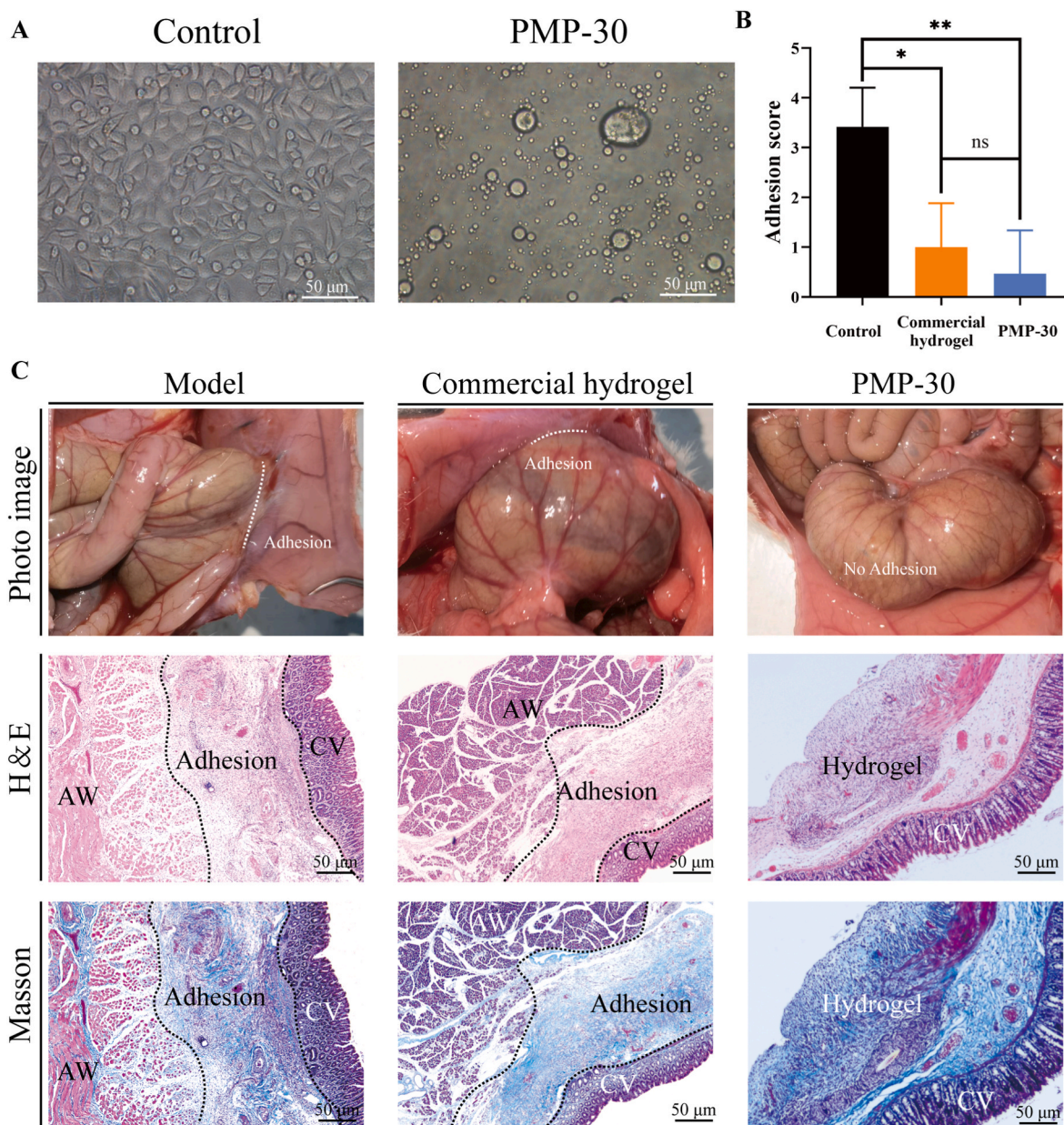


Fig. 6. *In vitro* and *in vivo* anti-adhesion of PMP-30. (A) Figures of the adhesion and growth of L929 cells on medium and PMP-30 hydrogel. (B) Image, H&E and Masson trichrome staining of postoperative anti-adhesion in rat injured abdominal wall-damaged cecum models treated with normal saline, commercial hydrogel, and PMP-30 14 days after surgery. CV refers to cecal villus, AW refers to abdominal wall. (C) Adhesion score of the model, commercial hydrogel, and PMP-30 groups. Data are presented as the mean \pm SD (n = 6). *P < 0.05, **P < 0.01, ***P < 0.001, and ns = no significance.

experiments.

3.9. *In vivo* hemostatic performance

Herein, rat liver injury model was utilized to evaluate the hemostatic capability of PMP-30 hydrogel, commercial gauze and gelatin sponge (GS) were used as control group. Fig. 8A presents photographic images of rat liver at the completion of hemostasis and 7 days after surgery. And the blood loss and hemostasis time recorded for the experiments are shown in Fig. 8B and C. Upon incision with a surgical blade, blood rapidly drains, saturating the underlying gauze. In the gauze group, effective hemostasis was unattainable without compression, the hemostasis time of the gauze group was 170 ± 29.24 s and the blood loss was 1249.2 ± 482.53 mg. GS could partially absorb the blood and accelerate hemostasis, however, blood still seepage persisted through the gap between GS and liver, yielding a hemostasis time of 100.2 ± 11.02 s and

blood loss of 1118.2 ± 233.03 mg. In contrast, PMP-30 hydrogel can effectively reduce blood flow after covering the wound, achieving complete hemostasis rapidly (41.5 ± 10.17 s), and resulting in minimal blood flow to the underlying gauze (596.2 ± 168.25 mg). This indicates the superior hemostatic properties of the PMP-30 hydrogel. Moreover, the hydrogel's rapid adhesion to the wound and subsequent closure also contribute to its hemostatic prowess.

At 7-day postoperative assessment, severe adhesion was observed between liver lobes in the gauze group, resulting in high adhesion score and difficulty in separation. Conversely, almost no adhesion appeared in PMP-30 group, with a significantly lower adhesion score than that of the gauze group (Fig. 8D). The substantial fibrin deposition and fibroblast proliferation following *in vivo* wound hemostasis can readily lead to unnecessary adhesion with other tissues and organs, causing patients additional discomfort. This issue may be exacerbated by the adhesive properties of some hydrogels. In our study, PMP-30 hydrogel initially

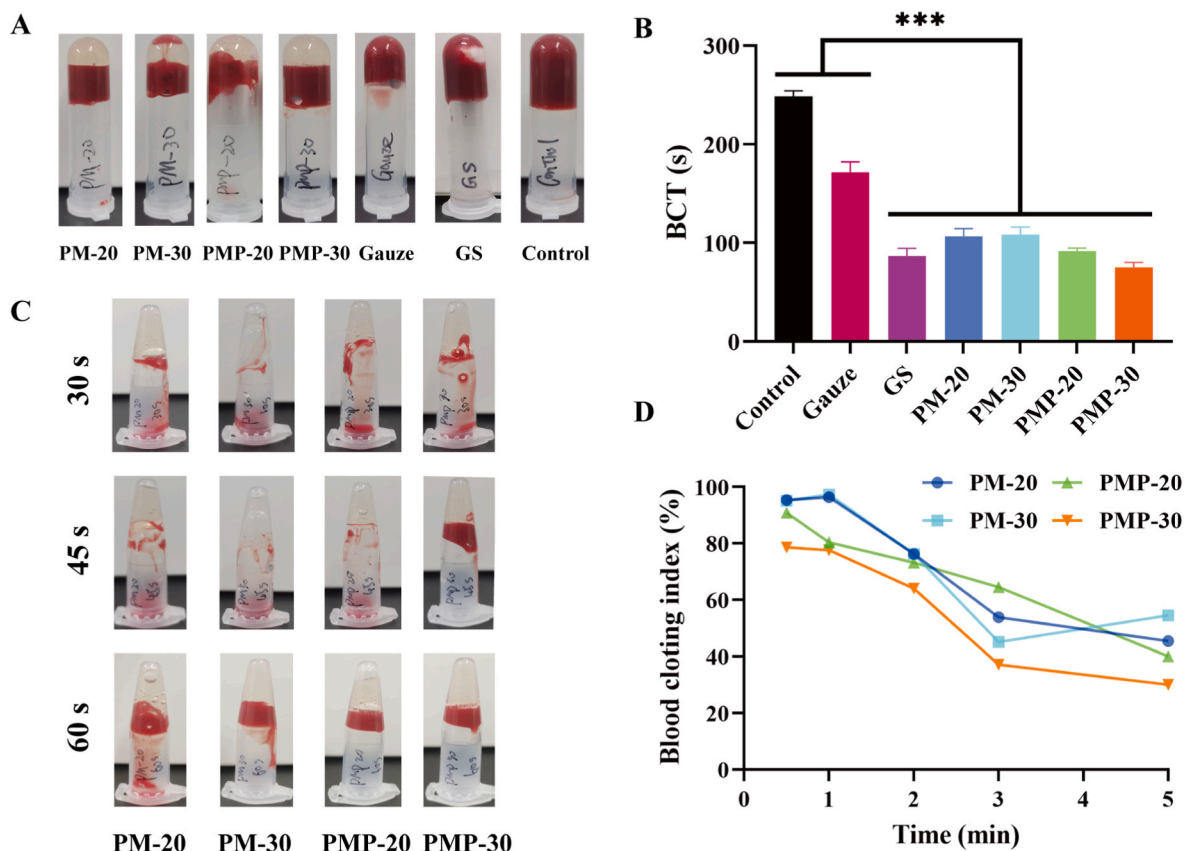


Fig. 7. *In vitro* blood clotting test of PM and PMP hydrogels. (A) Images and (B) Data of Blood Clotting Time tests. Data indicate the mean \pm SD ($n = 3$). (C) Images of liquid blood incubated with PM-20, PM-30, PMP-20 and PMP-30 within different seconds. (D) Data of *In vitro* BCI of PM-20, PM-30, PMP-20 and PMP-30. Data indicate the mean \pm SD ($n = 3$). * $P < 0.05$, ** $P < 0.01$, *** $P < 0.001$, and ns = no significance.

prevented excessive fibrinogen deposition at the wound site through rapid and effective hemostasis, thereby reducing potential for adhesion. Furthermore, PMP-30 hydrogel formed an anti-adhesion membrane structure after water treatment, which could protect and prevent against further tissue adhesions. This result was consistent with the previous experiment. Histopathological assessments of H&E as well as Masson trichrome staining showed that showed no tissue necrosis at the scratch site along with increased collagen fiber generation. The PMP-30 group demonstrated improved wound repair and a higher degree of healing compared to those treated with gauze alone. More fibrous tissue hyperplasia was observed in groups treated solely with gauze. Exogenous material may cause an inflammatory response, in GS group, foreign body giant cells were observed between incompletely degraded GS and tissues, and the undegraded GS would hinder further wound repair. No aggregation of foreign body giant cell was observed within those treated using PMP-30 hydrogel, which proved its excellent biocompatibility and biodegradability.

Four coagulation parameters, including APTT, TT, PT, and FIB, were further evaluated using rat plasma. As shown in Fig. 8E–H, the APTT and TT of PMP-30 group had no statistical difference compared with gauze group. However, a notable decrease in PT and an increase in FIB were observed (* $P < 0.01$). During hemorrhage, a cascade of coagulation factors is activated, culminating in a series of enzymatic reactions that convert soluble fibrinogen into insoluble fibrin, leading to clot formation [43]. The rats treated with PMP-30 hydrogel showed reduced PT and elevated FIB levels, suggesting the activation of fibrinogen system and the enhancement of hemostasis through the exogenous coagulation pathway [44]. Combined with the results of *in vitro* coagulation experiments, it can be inferred that the PMP-30 hydrogel initially obstructs the bleeding site to prevent further blood loss. Moreover, it activates the

exogenous coagulation cascade by enriching coagulation factors, facilitating the rapid conversion of fibrinogen to fibrin, and ultimately promoting hemostasis.

The hemostatic effect of the materials was further substantiated by a rat femoral artery injury model. As shown in Fig. S4, the high blood pressure at the wound site led to rapid blood spattering, making hemostasis challenging with gauze alone. A single gelatin sponge quickly became saturated with blood, requiring multiple replacements of gelatin sponge to achieve wound closure and total hemostasis. In contrast, PMP-30 hydrogel significantly shortened the hemostasis time. Upon injection into the wound, PMP-30 hydrogel rapidly engaged the bleeding site with minimal blood exudation observed at its periphery. Hemorrhage was promptly arrested without compromising the integrity of the PMP-30 hydrogel matrix.

The hemostatic experiment *in vivo* confirmed that PMP-30 hydrogel effectively promoted hemostasis by initially sealing wounds and preventing blood flow. Furthermore, hydrophilic end groups exposed by the dissociation of hydrogen bonds from both Gel and PMP can form new cooperative bonds with the groups on the adhesive surface, thereby enhancing the adhesion of the hydrogel. The enriched red blood cells and platelets would further promote the coagulation cascade to achieve hemostasis [45,46]. Additionally, PMP hydrogels activate the extrinsic coagulation cascade, accelerating the conversion of fibrinogen to fibrin, thereby facilitating rapid hemostasis at the wound site.

Due to the injectability and film-forming properties of PMP-30 hydrogel, the material can be administered to the surface of deep tissues or organs to address incompressible bleeding. The high biocompatibility, sustained anti-adhesion properties and non-toxic degradation of the material ensure its reliability as a hemostatic material. The mechanical properties of hydrogels are paramount for augmenting their

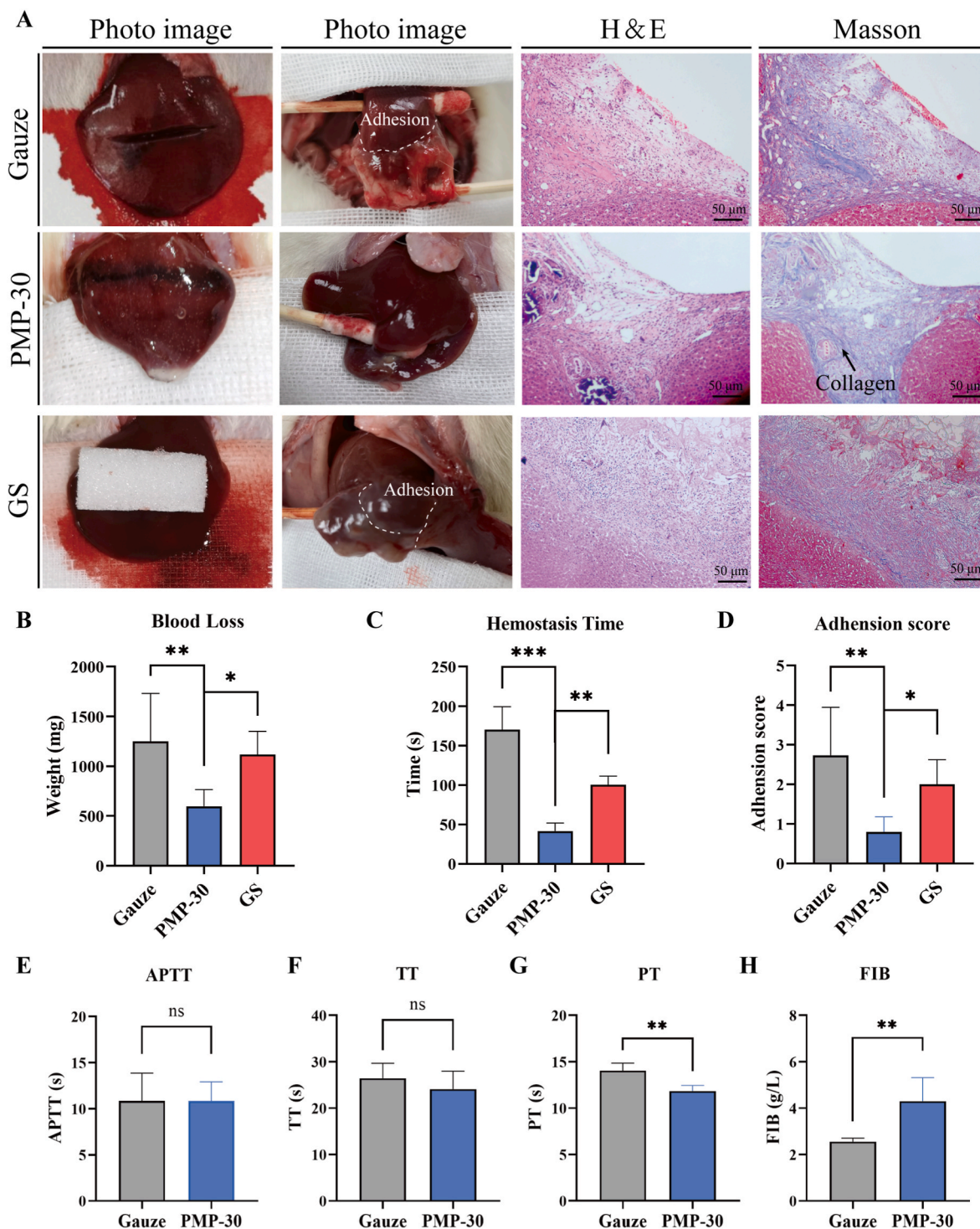


Fig. 8. Hemostatic performance of rat liver injury model. (A) Gross images, H&E and Masson trichrome staining of rat liver after injury and 7 days post-surgery. (B) Blood loss weight of liver after treatment with gauze, PMP-30 hydrogel and gelatin sponge. (C) Hemostasis time of the wound. (D) Adhesion score data indicate the mean \pm SD (n = 6); (E) Activated Partial Thromboplastin Time (APTT). (F) Thrombin Time (TT). (G) Prothrombin Time (PT). (H) Fibrinogen (FIB). Data indicate the mean \pm SD (n = 6). *P < 0.05, **P < 0.01, ***P < 0.001, and ns = no significance.

stability and therapeutic efficacy [47]. In scenarios requiring sustained hemostasis, it is imperative that hydrogels enhance their mechanical strength while maintaining effective hemostatic properties to endure the challenges posed by internal (blood flow) and external (movement or impact) pressures [48]. While the current mechanical properties of our material are sufficient to meet initial hemostasis requirements, further enhancement of its cohesiveness and toughness is necessary to extend its application to larger animals or wounds with significant bleeding. This

can be achieved by constructing double-network, interpenetrating network, and nanocomposite network structures to augment the overall mechanical strength of the hydrogel [49]. Otherwise, the structural failure of hemostatic materials often leads to hemostasis failure. The mechanical resistance of hemostatic materials to hemodynamic pressures can be further characterized using methods such as burst pressure testing. Moreover, hydrogels will be further engineered to serve as drug delivery vehicles for a spectrum of therapeutic applications,

encompassing antimicrobial, anti-inflammatory, and tissue repair interventions [50].

4. Conclusion

In summary, we have successfully synthesized a novel hemostatic material for incompressible bleeding and subsequent anti-adhesion *in vivo*. This material is a hydrophobic PLA chain that has been modified with hydrophilic PEG and anti-protein zwitterionic sulfobetaine, which spontaneously assemble into micelles in aqueous environments. PMP-30 was formulated by blending the modified PLA with gelatin and urea. The hydrogel demonstrated adaptability to conform complex irregular wounds and effective adhesion to the tissue surface under wet environments. After simple treatment of the surface of the hydrogel with water, the hydrophobic chain segments in the hydrogel formed a unique smooth anti-adhesion structure on the surface. The anti-protein adsorption ability of sulfonate betaine also prevented the abnormal adhesion of the hydrogel to the cavity walls and tissues when used *in vivo*. Notably, PMP-30 demonstrated superior anti-adhesion effect than commercially available hydrogel products. It was also effective in rapidly addressing pre-hospital treatment of incompressible hemorrhage, as well as performs well in multiple hemorrhage models with excellent hemostatic ability. Collectively, our hydrogel material emerges as a competitive hemostatic/anti-adhesion product capable of simultaneously addressing incompressible bleeding and subsequent adhesion issues *in vivo* without necessitating more complex procedures. Its potential application can be further explored across various clinical settings.

CRedit authorship contribution statement

Xinran Yang: Writing – original draft, Visualization, Data curation, Conceptualization. **Xiudan Wang:** Methodology, Data curation, Conceptualization. **Lizong Tang:** Validation, Formal analysis. **Zhi-guang Sun:** Validation, Investigation. **Xing Gao:** Validation, Resources, Investigation. **Yanmei Zhao:** Supervision, Resources. **Shike Hou:** Supervision, Resources, Methodology. **Jie Shi:** Writing – review & editing, Methodology. **Qi Lv:** Writing – review & editing, Supervision, Methodology.

Declaration of competing interest

The authors declare that they have no known competing financial interests or personal relationships that could have appeared to influence the work reported in this paper.

Acknowledgements

The authors are very thankful for financial support by National Key R&D Program of China (Grant 2022YFC3006200), Tianjin Natural Science Foundation (20JCYBJC01240), the Opening Project of Military Logistics (No. BLB20J009) and Scientific Research Translational Foundation of Wenzhou Safety (Emergency) Institute of Tianjin University (TJUWYY2022008, TJUWYY2022020).

Appendix A. Supplementary data

Supplementary data to this article can be found online at <https://doi.org/10.1016/j.mtbio.2024.101431>.

Data availability

No data was used for the research described in the article.

References

- [1] D.S. Kauvar, R. Lefering, C.E. Wade, Impact of hemorrhage on trauma outcome: an overview of epidemiology, clinical presentations, and therapeutic considerations, *J. Trauma Acute Care Surg.* 60 (2006) 6, <https://doi.org/10.1097/01.ta.0000199961.02677.19>.
- [2] S. Jiang, S. Liu, S. Lau, J. Li, Hemostatic biomaterials to halt non-compressible hemorrhage, *J. Mater. Chem. B* 10 (2022) 37, <https://doi.org/10.1039/D2TB00546H>.
- [3] L. Zhang, M. Liu, Y. Zhang, R. Pei, Recent progress of highly adhesive hydrogels as wound dressings, *Biomacromolecules* 21 (2020) 10, <https://doi.org/10.1021/acs.biomac.0c01069>.
- [4] G. Pan, F. Li, S. He, W. Li, Q. Wu, J. He, R. Ruan, Z. Xiao, J. Zhang, H. Yang, Mussel- and barnacle cement proteins-inspired dual-bionic bioadhesive with repeatable wet-tissue adhesion, multimodal self-healing, and antibacterial capability for nonpressing hemostasis and promoted wound healing, *Adv. Funct. Mater.* 32 (2022) 25, <https://doi.org/10.1002/adfm.202200908>.
- [5] Z. Chen, H. Wu, H. Wang, D. Zaldivar-Silva, L. Aguero, Y. Liu, Z. Zhang, Y. Yin, B. Qiu, J. Zhao, X. Lu, S. Wang, An injectable anti-microbial and adhesive hydrogel for the effective noncompressible visceral hemostasis and wound repair, *Mater. Sci. Eng., C* 129 (2021), <https://doi.org/10.1016/j.msec.2021.112422>.
- [6] C. Liu, C. Liu, Z. Liu, Z. Shi, S. Liu, X. Wang, X. Wang, F. Huang, Injectable thermogelling bioadhesive chitosan-based hydrogels for efficient hemostasis, *Int. J. Biol. Macromol.* 224 (2023), <https://doi.org/10.1016/j.ijbiomac.2022.10.194>.
- [7] X. Wang, X. Zhang, X. Yang, X. Guo, Y. Liu, Y. Li, Z. Ding, Y. Teng, S. Hou, J. Shi, Q. Lv, An antibacterial and antiadhesion in situ forming hydrogel with sol-spray system for noncompressible hemostasis, *ACS Appl. Mater. Interfaces* 15 (2023) 1, <https://doi.org/10.1021/acsami.2c19662>.
- [8] L.S. Nair, C.T. Laurencin, *Polymers as biomaterials for tissue engineering and controlled drug delivery*, in: K. Lee, D. Kaplan (Eds.), *Tissue Engineering I*, Springer Berlin Heidelberg, Berlin, Heidelberg, 2006, pp. 47–90.
- [9] A.M. Haaparanta, E. Järvinen, I.F. Cengiz, V. Ellä, H.T. Kokkonen, I. Kiviranta, M. Kellomäki, Preparation and characterization of collagen/PLA, chitosan/PLA, and collagen/chitosan/PLA hybrid scaffolds for cartilage tissue engineering, *J. Mater. Sci. Mater. Med.* 25 (2014) 4, <https://doi.org/10.1007/s10856-013-5129-5>.
- [10] S. Liu, G. Wu, X. Chen, X. Zhang, J. Yu, M. Liu, Y. Zhang, P. Wang, Degradation behavior in vitro of carbon nanotubes (CNTs)/Poly(lactic acid) (PLA) composite suture, *Polymers* 11 (2019) 6, <https://doi.org/10.3390/polym11061015>.
- [11] G. Li, M. Zhao, F. Xu, B. Yang, X. Li, X. Meng, L. Teng, F. Sun, Y. Li, *Synthesis and biological application of poly(lactic acid)*, *Molecules* 25 (2020) 21.
- [12] S. Chen, J. Zheng, L. Li, S. Jiang, Strong resistance of phosphorylcholine self-assembled monolayers to protein adsorption: insights into nonfouling properties of zwitterionic materials, *J. Am. Chem. Soc.* 127 (2005) 41, <https://doi.org/10.1021/ja054169u>.
- [13] S. Jiang, Z. Cao, Ultralow-fouling, functionalizable, and hydrolyzable zwitterionic materials and their derivatives for biological applications, *Adv. Mater.* 22 (2010) 9, <https://doi.org/10.1002/adma.200901407>.
- [14] Q. Tu, J.-C. Wang, R. Liu, Y. Zhang, J. Xu, J. Liu, M.-S. Yuan, W. Liu, J. Wang, Synthesis of polyethylene glycol- and sulfobetaine-conjugated zwitterionic poly(l-lactide) and assay of its antifouling properties, *Colloids Surf. B Biointerfaces* 102 (2013), <https://doi.org/10.1016/j.colsurfb.2012.08.025>.
- [15] G. Yang, Z. Xiao, H. Long, K. Ma, J. Zhang, X. Ren, J. Zhang, Assessment of the characteristics and biocompatibility of gelatin sponge scaffolds prepared by various crosslinking methods, *Sci. Rep.* 8 (2018) 1, <https://doi.org/10.1038/s41598-018-20006-y>.
- [16] K. Xu, Y. Fu, W. Chung, X. Zheng, Y. Cui, I.C. Hsu, W.J. Kao, Thiol-ene-based biological/synthetic hybrid biomatrix for 3-D living cell culture, *Acta Biomater.* 8 (2012) 7, <https://doi.org/10.1016/j.actbio.2012.03.049>.
- [17] X. Su, W. Xie, P. Wang, Z. Tian, H. Wang, Z. Yuan, X. Liu, J. Huang, Strong underwater adhesion of injectable hydrogels triggered by diffusion of small molecules, *Mater. Horiz.* 8 (2021) 8, <https://doi.org/10.1039/D1MH00533B>.
- [18] A. Narayanan, Y. Xu, A. Dhinojwala, A. Joy, *Advances in photoreactive tissue adhesives derived from natural polymers*, *ChemEngineering* 4 (2020) 2.
- [19] S. Ishikawa, D. Matsukuma, K. Iijima, M. Iijima, S. Osawa, H. Otsuka, N-hydroxysuccinimide bifunctionalized triblock cross-linker having hydrolysis property for a biodegradable and injectable hydrogel system, *ACS Biomater. Sci. Eng.* 5 (2019) 11, <https://doi.org/10.1021/acsbomaterials.9b00218>.
- [20] X. Zhao, P. Li, B. Guo, P.X. Ma, Antibacterial and conductive injectable hydrogels based on quaternized chitosan-graft-polyaniline/oxidized dextran for tissue engineering, *Acta Biomater.* 26 (2015), <https://doi.org/10.1016/j.actbio.2015.08.006>.
- [21] J.H. Ryu, Y. Lee, W.H. Kong, T.G. Kim, T.G. Park, H. Lee, Catechol-functionalized chitosan/pluronic hydrogels for tissue adhesives and hemostatic materials, *Biomacromolecules* 12 (2011) 7, <https://doi.org/10.1021/bm200464x>.
- [22] Y. Hu, L. Barbier, Z. Li, X. Ji, H. Le Blay, D. Hourdet, N. Sanson, J.W.Y. Lam, A. Marcellan, B.Z. Tang, Hydrophilicity-hydrophobicity transformation, thermoresponsive morphomechanics, and crack multifurcation revealed by AIEgens in mechanically strong hydrogels, *Adv. Mater.* 33 (2021) 39, <https://doi.org/10.1002/adma.202101500>.
- [23] Z. Li, Y. Zhao, X. Ouyang, Y. Yang, Y. Chen, Q. Luo, Y. Zhang, D. Zhu, X. Yu, L. Li, Biomimetic hybrid hydrogel for hemostasis, adhesion prevention and promoting regeneration after partial liver resection, *Bioact. Mater.* 11 (2022).
- [24] W. Huang, S. Cheng, X. Wang, Y. Zhang, L. Chen, L. Zhang, Noncompressible hemostasis and bone regeneration induced by an absorbable bioadhesive self-

- healing hydrogel, *Adv. Funct. Mater.* 31 (2021) 22, <https://doi.org/10.1002/adfm.202009189>.
- [25] Z. Zhu, K. Zhang, Y. Xian, G. He, Z. Pan, H. Wang, C. Zhang, D. Wu, A choline phosphoryl-conjugated chitosan/oxidized dextran injectable self-healing hydrogel for improved hemostatic efficacy, *Biomacromolecules* 24 (2023) 2, <https://doi.org/10.1021/acs.biomac.2c01143>.
- [26] X. Wei, C. Cui, C. Fan, T. Wu, Y. Li, X. Zhang, K. Wang, Y. Pang, P. Yao, J. Yang, Injectable hydrogel based on dodecyl-modified N-carboxyethyl chitosan/oxidized konjac glucomannan effectively prevents bleeding and postoperative adhesions after partial hepatectomy, *Int. J. Biol. Macromol.* 199 (2022), <https://doi.org/10.1016/j.ijbiomac.2021.12.193>.
- [27] F. Cheng, C. Liu, X. Wei, T. Yan, H. Li, J. He, Y. Huang, Preparation and characterization of 2, 2, 6, 6-tetramethylpiperidine-1-oxyl (TEMPO)-oxidized cellulose nanocrystal/alginate biodegradable composite dressing for hemostasis applications, *ACS Sustain. Chem. Eng.* 5 (2017) 5.
- [28] J. Li, X. Sun, K. Zhang, G. Yang, Y. Mu, C. Su, J. Pang, T. Chen, X. Chen, C. Feng, Chitosan/diatom-biosilica aerogel with controlled porous structure for rapid hemostasis, *Adv. Healthcare Mater.* 9 (2020) 21.
- [29] B. Yang, C. Gong, X. Zhao, S. Zhou, Z. Li, X. Qi, Q. Zhong, F. Luo, Z. Qian, Preventing postoperative abdominal adhesions in a rat model with PEG-PCL-PEG hydrogel, *Int. J. Nanomed.* 7 (2012) 547–557.
- [30] H. Li, X. Wei, X. Yi, S. Tang, J. He, Y. Huang, F. Cheng, Antibacterial, hemostasis, adhesive, self-healing polysaccharides-based composite hydrogel wound dressing for the prevention and treatment of postoperative adhesion, *Mater. Sci. Eng. C* 123 (2021), <https://doi.org/10.1016/j.msec.2021.111978>.
- [31] C. Cui, C. Fan, Y. Wu, M. Xiao, T. Wu, D. Zhang, X. Chen, B. Liu, Z. Xu, B. Qu, W. Liu, Water-triggered hyperbranched polymer universal adhesives: from strong underwater adhesion to rapid sealing hemostasis, *Adv. Mater.* 31 (2019) 49, <https://doi.org/10.1002/adma.201905761>.
- [32] J. Chen, L. Qiu, Q. Li, J. Ai, H. Liu, Q. Chen, Rapid hemostasis accompanied by antibacterial action of calcium crosslinking tannic acid-coated mesoporous silica/silver Janus nanoparticles, *Mater. Sci. Eng., C* 123 (2021), <https://doi.org/10.1016/j.msec.2021.111958>.
- [33] F. Chen, X. Cao, X. Chen, J. Wei, C. Liu, Calcium-modified microporous starch with potent hemostatic efficiency and excellent degradability for hemorrhage control, *J. Mater. Chem. B* 3 (2015) 19, <https://doi.org/10.1039/C5TB00250H>.
- [34] O. Laput, I. Vasenina, M.C. Salvadori, K. Savkin, D. Zuza, I. Kurzina, Low-temperature plasma treatment of polylactic acid and PLA/HA composite material, *J. Mater. Sci.* 54 (2019) 17, <https://doi.org/10.1007/s10853-019-03693-4>.
- [35] Y. Huang, M. Zhong, Y. Huang, M. Zhu, Z. Pei, Z. Wang, Q. Xue, X. Xie, C. Zhi, A self-healable and highly stretchable supercapacitor based on a dual crosslinked polyelectrolyte, *Nat. Commun.* 6 (2015) 1, <https://doi.org/10.1038/ncomms10310>.
- [36] Y. Wu, Y. Shi, H. Wang, Urea as a hydrogen bond producer for fabricating mechanically very strong hydrogels, *Macromolecules* 56 (2023) 12, <https://doi.org/10.1021/acs.macromol.3c00611>.
- [37] D. Du, X. Chen, C. Shi, Z. Zhang, D. Shi, D. Kaneko, T. Kaneko, Z. Hua, Mussel-inspired epoxy bioadhesive with enhanced interfacial interactions for wound repair, *Acta Biomater.* 136 (2021), <https://doi.org/10.1016/j.actbio.2021.09.054>.
- [38] Q. Ou, Y. Miao, F. Yang, X. Lin, L.-M. Zhang, Y. Wang, Zein/gelatin/nanohydroxyapatite nanofibrous scaffolds are biocompatible and promote osteogenic differentiation of human periodontal ligament stem cells, *Biomater. Sci.* 7 (2019) 5, <https://doi.org/10.1039/C8BM01653D>.
- [39] H. Sun, L. Yan, R. Zhang, J.F. Lovell, Y. Wu, C. Cheng, A sulfobetaine zwitterionic polymer–drug conjugate for multivalent paclitaxel and gemcitabine co-delivery, *Biomater. Sci.* 9 (2021) 14, <https://doi.org/10.1039/D1BM00393C>.
- [40] W. Du, H. Wei, T. Zhu, S. Zhang, Combination of ring-opening polymerization and “click” chemistry towards functionalization of polycaprolactone with sulfobetaine groups, *Polymer* 294 (2024), <https://doi.org/10.1016/j.polymer.2024.126721>.
- [41] V. Krishnadoss, A. Melillo, B. Kanjilal, T. Hannah, E. Ellis, A. Kapetanakis, J. Hazelton, J. San Roman, A. Masoumi, J. Leijten, I. Noshadi, Bioionic liquid conjugation as universal approach to engineer hemostatic bioadhesives, *ACS Appl. Mater. Interfaces* 11 (2019) 42, <https://doi.org/10.1021/acsami.9b08757>.
- [42] J. Park, T.Y. Kim, Y. Kim, S. An, K.S. Kim, M. Kang, S.A. Kim, J. Kim, J. Lee, S.-W. Cho, J. Seo, A mechanically resilient and tissue-conformable hydrogel with hemostatic and antibacterial capabilities for wound care, *Adv. Sci.* 10 (2023) 30, <https://doi.org/10.1002/advs.202303651>.
- [43] S. Pourshahrestani, E. Zeimaran, N.A. Kadri, N. Mutlu, A.R. Boccaccini, Polymeric hydrogel systems as emerging biomaterial platforms to enable hemostasis and wound healing, *Adv. Healthcare Mater.* 9 (2020) 20, <https://doi.org/10.1002/adhm.202000905>.
- [44] J. Luo, M. Zhang, J. Cheng, S. Wu, W. Xiong, H. Kong, Y. Zhao, H. Qu, Hemostatic effect of novel carbon dots derived from *Cirsium setosum* Carbonisata, *RSC Adv.* 8 (2018) 66, <https://doi.org/10.1039/C8RA06340K>.
- [45] Y. Huang, X. Zhao, Z. Zhang, Y. Liang, Z. Yin, B. Chen, L. Bai, Y. Han, B. Guo, Degradable gelatin-based IPN cryogel hemostat for rapidly stopping deep noncompressible hemorrhage and simultaneously improving wound healing, *Chem. Mater.* 32 (2020) 15, <https://doi.org/10.1021/acs.chemmater.0c02030>.
- [46] J. Zhu, F. Li, X. Wang, J. Yu, D. Wu, Hyaluronic acid and polyethylene glycol hybrid hydrogel encapsulating nanogel with hemostasis and sustainable antibacterial property for wound healing, *ACS Appl. Mater. Interfaces* 10 (2018) 16, <https://doi.org/10.1021/acsami.7b18927>.
- [47] X. Liang, L. Ding, J. Ma, J. Li, L. Cao, H. Liu, M. Teng, Z. Li, Y. Peng, H. Chen, Y. Zheng, H. Cheng, G. Liu, Enhanced mechanical strength and sustained drug release in carrier-free silver-coordinated anthraquinone natural antibacterial anti-inflammatory hydrogel for infectious wound healing, *Adv. Healthcare Mater.* 13 (2024) 23, <https://doi.org/10.1002/adhm.202400841>.
- [48] X. Yang, X. Wang, X. Gao, X. Guo, S. Hou, J. Shi, Q. Lv, What else should hemostatic materials do beyond hemostasis: a review, *Materials Today Bio* 25 (2024), <https://doi.org/10.1016/j.mtbio.2024.101008>.
- [49] S. Ge, Q. Liu, M. Li, J. Liu, H. Lu, F. Li, S. Zhang, Q. Sun, L. Xiong, Enhanced mechanical properties and gelling ability of gelatin hydrogels reinforced with chitin whiskers, *Food Hydrocolloids* 75 (2018), <https://doi.org/10.1016/j.foodhyd.2017.09.023>.
- [50] X. Liang, C. Huang, H. Liu, H. Chen, J. Shou, H. Cheng, G. Liu, Natural hydrogel dressings in wound care: design, advances, and perspectives, *Chin. Chem. Lett.* 35 (2024) 10, <https://doi.org/10.1016/j.ccllet.2023.109442>.